ACS APPLIED ENERGY MATERIALS

www.acsaem.org

Article

Impact of Thin Film Thickness on the Structural, Energetic and Optoelectronic Properties of Two-Dimensional $FPEA_2(MA_{n-1})Pb_nI_{3n+1}$ Perovskites

Israel C. Ribeiro, Felipe D. Picoli, Pedro Ivo R. Moraes, André F. V. Fonseca, Luiz N. Oliveira, Ana Flávia Nogueira, and Juarez L. F. Da Silva*

Cite This: https://doi.org/10.1021/acsaem.4c02800

Read Online

ACCESS | Metrics & More | Article Recommendations | Supporting Information

ABSTRACT: Perovskite solar cell devices, composed of solution-processed perovskite layers with thicknesses of a few hundred angstroms, represent a leading technology in thin-film photovoltaics. Here, we performed a theoretical investigation based on *ab initio* calculations to explore the role of perovskite thin film thickness, with the general formula $FPEA_2(MA_{n-1})Pb_nI_{3n+1}$, where FPEA represents 4-fluorophenylethylammonium cations and n ranges from 1 to 4 layers. Our findings reveal that increasing the thickness of the inorganic layer significantly influences the structural, energetic, and optoelectronic properties. Enhanced charge transfer within the inorganic framework and stronger organic−inorganic interactions are observed as the effective charge distribution shifts with increasing thickness. Exothermic trends in adsorption and interaction energies highlight the stabilizing effects of van der Waals forces and hydrogen bonding. The PbI_6-octahedra play a critical role in determining the optical activity and the formation of valence and conduction bands. Thicker films exhibit more intense absorption, emphasizing the importance of PbI_6-octahedra in driving optical properties. Moreover, the work function (ϕ) decreases with increasing thickness due to reduced quantum confinement effects, while the nature of polar FPEA molecules induces deviations in ϕ, underscoring the interaction between molecular composition and thickness. Band alignment further reveals strong spin−orbit coupling effects on the conduction band minimum (CBM), influenced by charge-transfer variability from FPEA to halides. These findings provide insights into thickness-dependent properties that are essential for optimizing perovskite-based devices.

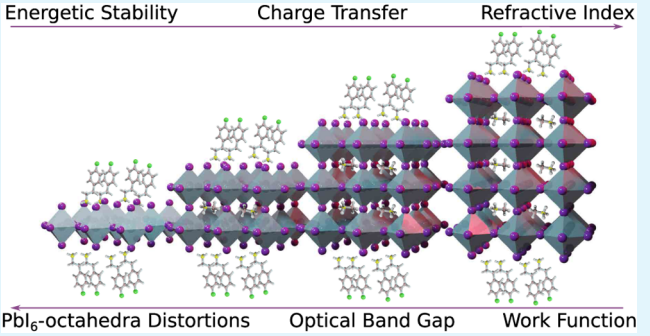

KEYWORDS: *perovskites thin films, quantum-size effects, $MAPbI_3$-based layers, 2D materials, DFT*

1. INTRODUCTION

Perovskite thin films have gained considerable attention in the past 15 years due to their easy and cost-effective synthesis and significant advancements in power conversion efficiency (PCE).[1,2] These materials, represented by the chemical formula ABX_3, crystallize in the perovskite structure, which consists of BX_6-octahedra, with divalent cations such as lead (Pb^{2+})[3] or tin (Sn^{2+})[4] at the *B*-site, and halide anions such as iodide (I^-)[5] or bromide (Br^-)[6] at the *X*-site. The *A*-site typically hosts monovalent cations, including methylammonium (MA^+),[7] formamidinium (FA^+),[8] cesium (Cs^+),[9] or a mixture of these.[10]

However, surface defects compromise the structural and electronic stability of the thin film, posing significant challenges for their large-scale application in perovskite-based solar cells (PSCs) devices.[11] In this context, passivation using long alkyl chain organic cations (*P*-cations), containing amines or aromatic ring substituted amines, has demonstrated significant effectiveness in enhancing the structural stability of perovskites, primarily due to the hydrophobic nature of these molecules.[12,13] During the passivation process with long-chain organic cations, low-dimensional structures can form beneath the perovskite surface. This results in films with varying thicknesses, such as two-dimensional (2D) perovskites.[14,15] The morphology of these films depends on the specific organic cation used. If monovalent *P*-cation type is present, these structures can adopt the Ruddlesden−Popper phase,[16] with the general chemical formula of $P_2(A_{n-1})B_nX_{n+1}$, where the n represents the number of inorganic layers (BX_6-octahedra).

The thickness of perovskite thin films plays a crucial role in their optoelectronic properties. For example, when n is 2 or

Received: November 2, 2024
Revised: February 26, 2025
Accepted: March 4, 2025

less, the exciton binding energy in these layered perovskites exceeds several hundred meV, preventing the efficient separation of charge carriers.[17] As n increases, a multilayered quasi-2D perovskite emerges, eventually transitioning to a three-dimensional (3D) structure when n approaches a very large number of layers. In this scenario, the exciton binding energy decreases as a function of increasing n. Thermodynamic and chemical constraints limit the achievable value n to obtain a pure quasi-2D phase, which typically results in structures with 3 to 7 BX_6-octahedra layers. In these cases, large organic cations fragment the 3D perovskite into isolated layers of corner-sharing BX_6-octahedra.[18,19]

Furthermore, Quan et al.[20] demonstrated through their experimental and theoretical investigations that perovskite thin films based on phenylethylammonium (PEA, $C_8H_9NH_3$) cations with low values of n exhibit greater stability in optical properties compared to those with higher values of n. However, devices with low thickness suffer from weak absorption and a larger bandgap, which negatively impacts performance. In contrast, at a higher number of layers, reduced charge-carrier mobility becomes the primary limitation, leading to significant radiative recombination losses. This suggests that 2D perovskite films with higher n values have the potential to achieve performance levels similar to those of 3D materials while also offering improved stability.

Therefore, investigations on the influence of the number of inorganic layers on the optoelectronic and structural properties are fundamental for the potential application of perovskite thin films in PSCs. Given this context, in this work, we report a theoretical investigation based on *ab initio* density functional theory (DFT) calculations[21,22] on $FPEA_2(MA_{n-1})Pb_nI_{3n+1}$ perovskite films with different thicknesses, exploring n from 1 to 4.

For *P*-cations, we have selected the 4-fluorophenylethylammonium (FPEA, $C_8H_{11}FN$) molecules. FPEAI, a fluorinated derivative of PEAI (the most widely used organic cation in the literature), builds on its properties by offering enhanced charge delocalization, reduced interlayer spacing, greater hydrophobicity, and increased polarization as a result of fluorination. These features improve charge separation, transport in PSCs, and strengthen interactions within the perovskite film, contributing to overall device stability.[23,24]

Our investigation demonstrates that the influence of thickness changes the characteristics of thin film perovskites, thereby providing a mechanism to modulate their properties. In particular, changes in the FPEA conformation corresponding to varying values of n have a pronounced impact on energetic stability, highlighting the complex interplay of structural factors within the inorganic framework. We found a trend in the energetic stability of the FPEA passivation as a function of thickness, with the adsorption and interaction energies of the organic cation decreasing as n increases. Furthermore, quantum confinement effects significantly impact the charge transfer dynamics from FPEA to PbI_6-octahedra, with larger slab thicknesses correlated with increased charge transfer. The crucial role of PbI_6-octahedra in optical activity highlights the importance of thoroughly understanding the impact of the number of inorganic layers in perovskites to fully grasp their optoelectronic performance.

2. THEORETICAL APPROACH AND COMPUTATIONAL DETAILS

2.1. Total Energy Calculations. Our calculations were based on the DFT[21,22] framework within the semilocal Perdew−Burke−Ernzerhof[25] (PBE) formulation for the exchange-correlation (XC) energy functional. Plain DFT-PBE can not provide an accurate description of long-range nonlocal van der Waals (vdW) interactions, which under estimates the interlayer binding energies among monolayers in 2D materials,[26] adsorption of molecular species on surfaces,[27] interactions of organic monovalent cations in the inorganic framework within hybrid perovskite,[28] etc. Thus, to minimize this problem, we used the semiempirical D3 vdW correction,[29] which provides an improved description at a lower computational cost. To describe the interactions among core−valence electrons, we used the frozen core projector augmented wave (PAW) method,[30,31] as implemented in the Vienna Ab initio Simulation Package (VASP),[32,33] version 5.4.4, where the KS orbitals are expanded in plane waves.

The chosen organic FPEA-cation for the passivation potentially influences the in-plane (xy) equilibrium lattice parameters (a_0, b_0). Consequently, to accommodate these variations, all equilibrium structures underwent optimization of the in-plane stress tensor and atomic forces,[34] using a plane wave cutoff energy of $1.50 \times ENMAX_{max}$, where $ENMAX_{max}$ represents the maximum recommended cutoff energy within PAW projectors specific to each atomic specie, for instance, 731.547 eV. During stress-tensor calculations, the magnitude of the stress tensor along the z-direction remained unchanged (maintained slab geometry). However, all atomic forces were optimized without constraints.

For the remaining properties, including adsorption and interaction energies, density of states (DOS), band structures, work function, absorption coefficient, net atomic charges computed by the density-derived electrostatic and chemical (DDEC) method[35,36] and so on, we used a plane wave cutoff energy of 548.660 eV in all systems, which is higher than the maximum recommended plane wave cutoff energy by 12.5%, taking into account all chosen PAW projectors. To sample the Brillouin zone (BZ), we employed a **k**-mesh of $2 \times 2 \times 1$ for structure optimization and $4 \times 4 \times 1$ for the remaining properties. The equilibrium structures were reached once the atomic forces in each atom fell below 2.50×10^{-2} eVÅ^{-1} and using a total energy convergence criterion of 10^{-5} eV.

2.2. Two-Dimensional Perovskite Thin Films. The passivation with long alkyl chain organic cations (*P*-cations) on perovskite surfaces induces the formation of low-dimensional structures, e.g., 2D perovskite thin films, in which due to the presence of a single NH_3^+ group, we have structures with general chemical formulas corresponding to the 2D Ruddlesden−Popper phase.[16] Here, our model can be visualized by envisioning a typical 3D perovskite crystal in the (100) direction, adopting a general formula of $FPEA_2(MA_{n-1})Pb_nI_{3n+1}$. The FPEA-cations serve as a passivating agent for ultrathin inorganic layers composed of PbI_6-octahedra, and the thickness of the slab is controlled by n layers, from 1 to 4 layers.

Thus, a 3D orthorhombic ($2 \times 2 \times 2$) supercell is employed to generate a (100) 2D surface slab with a vacuum thickness measuring 15 Å. Consequently, adhering to the electron counting rule, each side of the slab (top and bottom) necessitates 4 *P*-cations to achieve full surface passivation.

https://doi.org/10.1021/acsaem.4c02800
ACS Appl. Energy Mater. XXXX, XXX, XXX−XXX

These configurations are denoted as $P_8Pb_4I_{16}$ (n = 1, 1L), $P_8(MA)_4Pb_8I_{28}$ (n = 2, 2L), $P_8(MA)_8Pb_{12}I_{40}$ (n = 3, 3L), and $P_8(MA)_{12}Pb_{16}I_{52}$ (n = 4, 4L).

2.3. FPEA Adsorption on Perovskites Layers. The FPEA-cations have demonstrated high performance in reducing possible structural defects when used as a passivating agent in perovskite thin films.[37,38] For the FPEA adsorption, we considered the NH_3^+ oriented in the vertical (v), horizontal (h), and slant (s) relative to the plane PbI_2 to examine the interface dipole effects of the orientations of the headgroup, as illustrated in Figure 1.

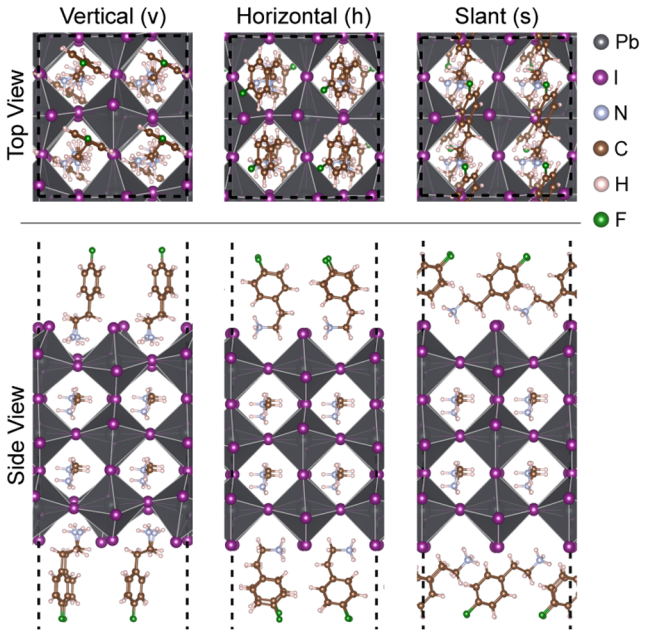

Figure 1. Top and side views of trial configurations for the vertical (v), horizontal (h), and slant (s) orientation of the NH_3^+ group to the PbI_2 plane, considering the 3L structure as example. The dashed line represents the unit cell.

The choice of systems with 1 to 4 layers was primarily driven by the computational challenge of performing DFT-PBE + D3 calculations with structural optimization using stress tensor and atomic forces, as demonstrated for thin films with 1 and 2 layers and different types of organic cations. In this way, a specific computational methodology was developed to reduce the optimization costs of these systems, which can be found elsewhere.[39]

In summary, the optimization process was initiated by keeping the in-plane lattice parameters (a_0, b_0) constant and fixing c_0, with selective dynamics allowing only the FPEA-cations to relax while constraining the inorganic slab. Calculations were performed using the Γ-point and a plane wave cutoff energy set to 426.736 eV. The system was subjected to an average of 300 ionic steps. Subsequent steps involved the refinement of force for all atoms, adjustments to the stress tensor, and increasing the cutoff energy to 731.547 eV. A final optimization step used a 2 × 2 × 1 **k**-mesh, yielding equilibrium lattice parameters. Further insights into geometric optimization methodologies are available in our previous publications.[39,40]

3. RESULTS AND DISCUSSION

In order to improve our understanding of the passivation effects induced by FPEA organic cations, referred to as *P*-cation, we conducted several characterizations that encompass structural, energetic, electronic and optical properties using various descriptors (physicochemical properties). In the following sections, we will underscore the key discoveries, while the supplementary data and analyses are available in the Supporting Information (SI) file.

3.1. Lowest Energy Configurations in Function of FPEA-Cation Orientation. To begin, we perform multiple stress tensor optimizations for the $FPEA_2(MA_{n-1})Pb_nI_{3n+1}$ perovskite thin films, applying different conformations to the FPEA molecule, Figure 1. For physicochemical characterizations, we focused on the structures with the lowest total energy, as shown in Figure 2.

To determine the structures with the lowest energy, we performed a relative energy (ΔE_{tot}) analysis. The results of ΔE_{tot} are shown in Figure 3, and we found, with the exception of the 1L system, that there is a convergence toward the h conformation as the lowest energy structure. The conformation of the FPEA molecule can induce large differences in the values of ΔE_{tot}, as seen for the structural s conformations for the 3L and 4L structures, since the FPEA···I interactions can be affected and thus reduce the stability of the system.

Intermolecular interactions such as hydrogen bonds (H-bonds) or dipole moments, as well as distortions along the

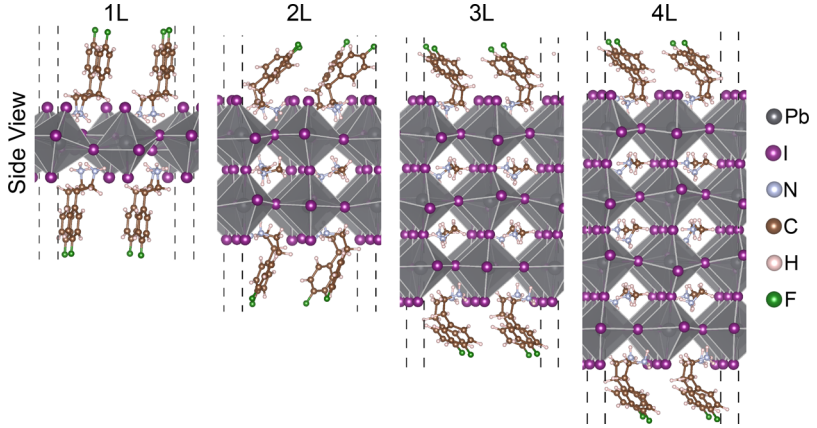

Figure 2. Side views for the lowest energy $FPEA_2(MA_{n-1})Pb_nI_{3n+1}$ perovskites thin films (n = 1 to 4 layers), considering an angle rotation of 8° on a_0 lattice parameter for better visualization. The dashed line represents the unit cell.

https://doi.org/10.1021/acsaem.4c02800
ACS Appl. Energy Mater. XXXX, XXX, XXX−XXX

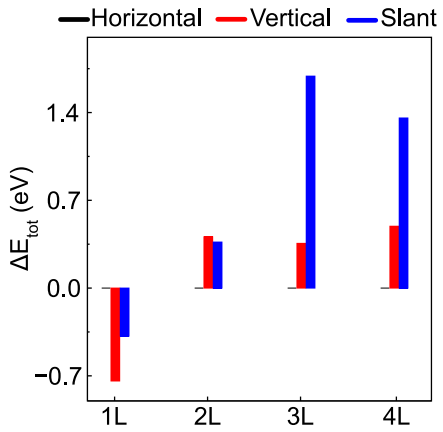

Figure 3. Relative total energy (ΔE_{tot}) for all configurations (*v*, *h*, and *s*) for the $FPEA_2(MA_{n-1})Pb_nI_{3n+1}$ perovskites thin films, with n = 1 to 4 layers. Here, the *h* orientations are at ΔE_{tot} = 0.

inorganic framework, have an impact on the energetic stability of 2D perovskite thin films.[41−43] The latter directly depends on the conformation of the organic cation. For example, FPEA molecules in the *s* conformation can induce a strong energy of repulsion between aromatic rings and thus contribute to an increase in the total energy.

The conformations of the organic cation FPEA might be affected by the dipole generated by the interlayer molecules (methylammonium (MA), CH_6N), such that the structural *v* conformation is favored in the 1L system. However, the inclusion of the MA cation results in a deviation of the NH_3^+ group from the FPEA conformation relative to the PbI_2 plane.

3.2. Role of *n*-Layers on Slab Lattice Deformations. To examine the influence of FPEA-cations on the slab lattice, we opted for two structural descriptors: (i) the equilibrium lattice parameters (a_0, b_0) and (ii) surface area (A_{cell}), in which the latter is defined as the product of the lattice parameters, that is, $a_0 \times b_0$. The findings are depicted in Figure 4.

The results indicate a significant influence of the number of layers on the values of b_0. Considering the lowest energy configurations, we found a deviation of 5.35% from 1L to 3L, with a nearly linear increase in b_0 corresponding to the increase in layers. Hence, primarily due to b_0, the quantity of inorganic layers impacts A_{cell}. Essentially, increasing the thickness of the FPEA-based perovskite thin films in a quantum well structure will decrease the quantum confinement, thus increasing A_{cell}.[44,45]

The lattice parameter a_0 alternately decreases in layers with odd numbers (1L and 3L) and increases in even-numbered ones (2L and 4L); this may be closely associated with the distinct symmetry effects between these systems. As shown in Figure 5, odd-numbered layers exhibit a pseudoinversion

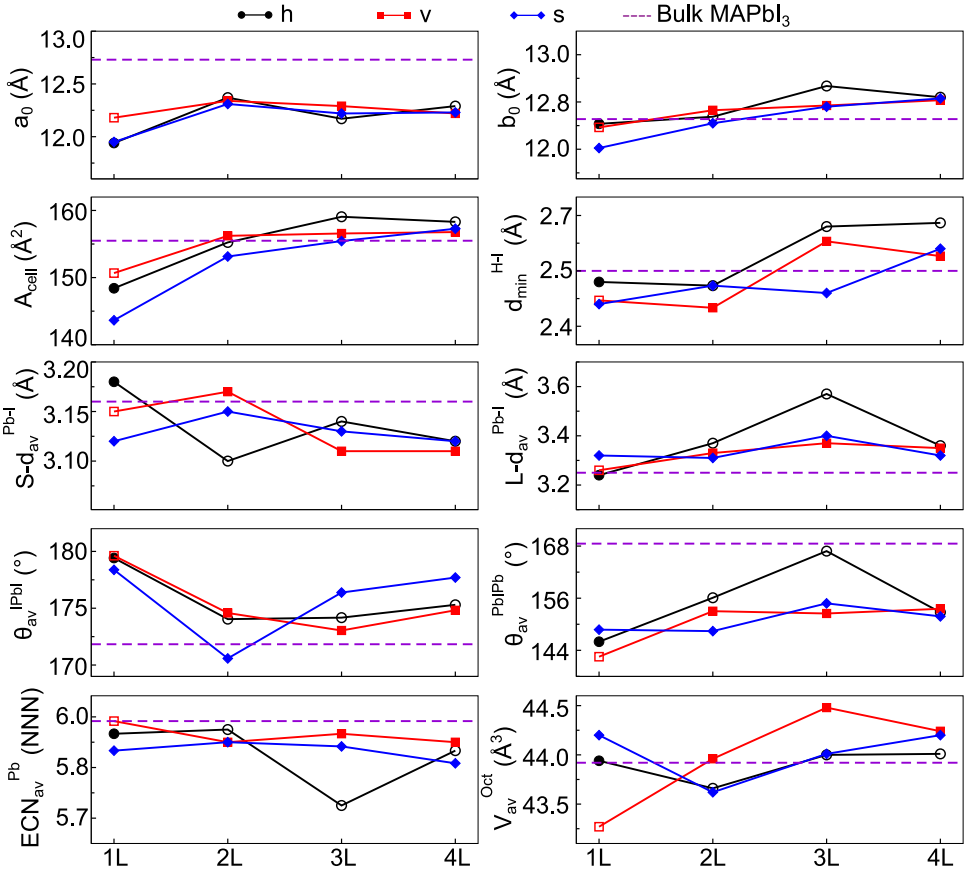

Figure 4. Equilibrium structural parameters for all initial configurations *h*, *v* and *s* for the $FPEA_2(MA_{n-1})Pb_nI_{3n+1}$ perovskites thin films, n = 1 to 4 layers, where the lowest energy conformations are represented by empty points: lattice parameters (a_0, b_0), surface unit cell area (A_{cell}), the average hydrogen bond distance with the iodine ($d_{av}^{H\cdots I}$), average bond distance of the short (S-d_{av}^{Pb-I}) and long (L-d_{av}^{Pb-I}) bonds, average angles for the I−Pb−I (θ_{av}^{IPbI}) and Pb−I−Pb (θ_{av}^{PbIPb}) combinations, the effective coordination number for the Pb (ECN_{av}^{Pb}) and the average volume of the PbI_6-octahedra (V_{av}^{Oct}).

https://doi.org/10.1021/acsaem.4c02800
ACS Appl. Energy Mater. XXXX, XXX, XXX−XXX

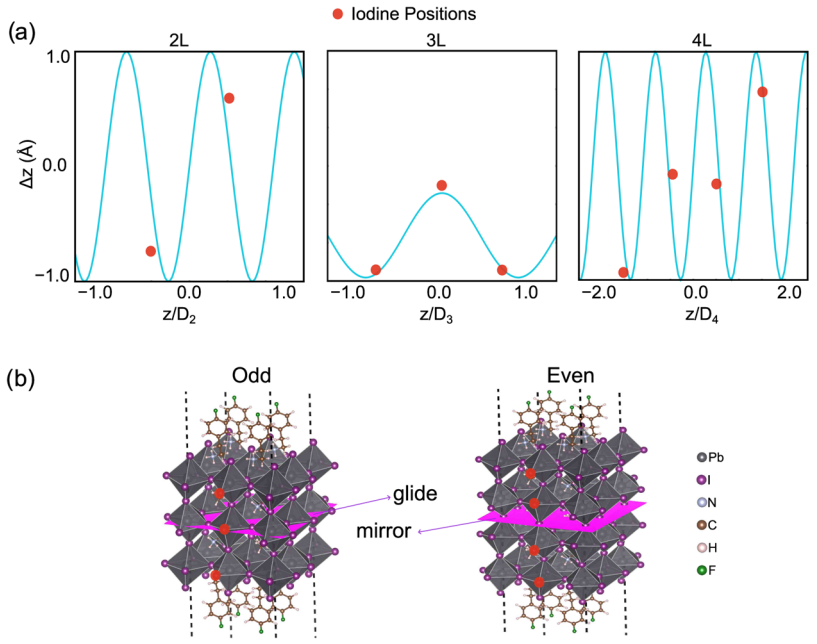

Figure 5. (a) Displacements of the equatorial iodine ions as a function of the distance from the glide (odd layers) or mirror (even layers) symmetry plane. The red circles show the displacements extracted from Table S4 in SI, and the solid blue lines represent eq 1 (2L and 4L) or eq 2 (3L). (b) In odd-numbered layers, a glide plane intersects the central layer, while in even-numbered layers, a mirror plane exists between the two middle perovskite networks, relating them to each other.

symmetry characterized by a glide plane passing through the central layer, which could lead to a more compact structure, resulting in a lower value a_0.

Conversely, even-numbered layers, which lack inversion symmetry and are related by a mirror plane bisecting the layers, may adopt a more expanded structure, leading to an increase in a_0. These symmetry-related effects play a significant role in defining the structural and lattice properties, contributing to the systematic variation in the lattice parameter observed in these perovskite systems and in other examples of 2D perovskites with different organic cations.[18]

3.3. PbI_6−Octahedra Distortions. To improve structural analysis, the following local geometric parameters were chosen: (i) mean lengths of bonds and angles within PbI_6-octahedra, (ii) average effective coordination numbers for Pb (ECN_{av}^{Pb}), and (iii) average volume of PbI_6-octahedra (V_{av}^{oct}). The results are depicted in Figure 4, with further elaboration provided in the subsequent discussion of the data.

The results reveal minimal deviations in the Pb−I chemical bonds contingent on the number of layers, manifesting both short (S-d_{av}^{Pb-I}) and long (L-d_{av}^{Pb-I}) bonds. However, there is no discernible evidence of Jahn−Teller-type distortions;[46] i.e., there is no presence of bond lengthening and shortening. An almost linear increase in L-d_{av}^{Pb-I} bonds is evident, attributable to the cumulative effect of Pb−I bonds along the c_0 direction, which tends to increase with the layer count.

The distortions of PbI_6-octahedra are determined to be out-of-phase,[47] and can be characterized by the bond angles for the I−Pb−I (θ_{av}^{IPbI}) and Pb−I−Pb (θ_{av}^{PbIPb}), Figure 4. The 1L system exhibits the highest θ_{av}^{IPbI} value, approximately 180°, indicative of the internal bond angles within the PbI_6-octahedra. With an increase in the number of inorganic layers, the θ_{av}^{IPbI} angles decrease, reflecting greater distortion effects along the z-axis due to increased interactions between layers. Specifically, noticeable distortions manifest at the θ_{av}^{PbIPb} angles in the 1L system, showcasing pronounced out-of-phase distortions compared to systems with higher n. This observation underscores the significant impact of quantum confinement in 1L systems, which results in increased distortions. Moreover, as the thickness increases, the θ_{av}^{PbIPb} values tend to approach those observed in the 3D bulk $MAPbI_3$, demonstrating a convergence toward the bulk behavior.

The characterizations of the effective coordination number for Pb (ECN_{av}^{Pb}) align with observations of internal distortions within the PbI_6-octahedra. Small deviations in ECN_{av}^{Pb} are contingent upon the thickness of the system, indicating minimal deformations along the Pb−I bonds. However, the observed trend in the L-d_{av}^{Pb-I} values reveals a progressive expansion in the volume of the PbI_6-octahedra (V_{av}^{Oct}) relative to the number of inorganic layers, ultimately converging toward values similar to those identified in the 3D bulk $MAPbI_3$.

To delve deeper into the physical implications of the multilayer structure, we now examine it from a different perspective. If periodic boundary conditions could be applied in the direction of the c_0, the z dependence of the wave functions would be subject to Bloch's theorem, and the local physical properties would be spatially periodic in that direction. The thin film geometry is, of course, compatible with open boundary conditions only, a restriction that invalidates the theorem. However, certain consequences of Bloch's statement are expected to survive in a modified form.

To verify this reasoning, consider the displacements Δz along the c_0 of the equatorial iodine ions in the thin films from their ideal positions in the three-dimensional compound. The Table S4 on SI file lists the displacements of positions I_j and I_j' (j = 1, ···, N_l) in the unit cell for the N_l = 2, 3, and 4 layers, where I_j' corresponds to the adjacent iodine.

Inspection of Table S4 shows that, both at positions I_j and I_j', the displacements are (approximately) antisymmetric with respect to the mirror plane for an even number of layers (2L

https://doi.org/10.1021/acsaem.4c02800
ACS Appl. Energy Mater. XXXX, XXX, XXX−XXX

and 4L), and symmetric with respect to the glide plane for three layers (3L), see Figure 5. The displacement is therefore an odd eigenvector of the z-inversion operator for two or four layers, while it is an even eigenvector for three layers. The results also show that the displacements of each I_j ion and the corresponding I_j' ion have opposite signs. In the 2L and 4L systems, the said displacements are moreover antisymmetric; it suffices to study the I_j ions. In the 3L films, there is no antisymmetry, and the I_j and I_j' should be considered separately. For brevity, we will discuss the displacement of I_j' ions, which poses a more difficult challenge.

Given the loose connection with Bloch's theorem, we now attempt to describe the displacements as periodic functions of the ideal ionic positions along the c_0, measured from the plane of symmetry. In the four-layer film, the ideal positions, measured from the mirror plane, are

$$z_j = \frac{\mathcal{D}_4}{2} j \quad (j = \pm 1, \pm 3) \tag{1}$$

where $\mathcal{D}_4$ is the separation between neighboring layers. For the two-layer film, an analogous equality is maintained, with $\mathcal{D}_2$ substituted for $\mathcal{D}_4$, and j ranging from -1 to 1.

Since the parity eigenvectors are odd for two or four layers, the odd trigonometric function is appropriate

$$\Delta z_j = \sin\left(\frac{2\pi z_j}{\lambda_n}\right) \quad (n = 2, 4) \tag{2}$$

Although an amplitude might be introduced as an adjustable parameter, simplicity recommends a unitary amplitude, given that the displacements in Table S4 are of the order of 1 Å. This leaves a single adjustable parameter, the wavelength λ_n, measured in units of the interlayer separation $\mathcal{D}_n$ (n = 2 or 4). For the three-layer film, eq 1 becomes

$$z_j = \mathcal{D}_3 j \quad (j = 0, \pm 1) \tag{3}$$

where $\mathcal{D}_3$ denotes the interlayer splitting.

In this case, the parity eigenvector is even with respect to the $j \leftrightarrow -j$ inversion. The eigenfunctions may therefore be constant or even functions of z_j. This considered, notice taken that $\Delta z \approx 0$ for the $I_{j=2}$ ion, we rely on the following equality to describe the displacement of the I_j ions

$$\Delta z_j = -\sin^2\left(\frac{2\pi z_j}{\lambda_3}\right) \quad (j = 0, \pm 1) \tag{4}$$

with a negative sign because the pertinent displacements in Table S4 are negative. The sign is arbitrary, since it reflects the orientation of the z-axis.

The solid blue curves in Figure 5 represent the best fit to the red circles, which correspond to the displacements listed in Table S4, with fitting parameters $\lambda_2 = 1.1\mathcal{D}_2$ for 2L, $\lambda_3 = 2.2\mathcal{D}_3$ for 3L and $\lambda_4 = 1.1\mathcal{D}_4$ for 4L. Although the quality of the fit, achieved using a single adjustable parameter for each case, is notable, the key insight lies in the conclusions drawn from these plots. Equations 2 and 4 describe displacement waves that lock onto the film structure, with wavelengths that approximately match the spacing between even-numbered layers or the outermost layers in odd-numbered. These waves, likely driven by the repulsion between iodine ions, introduce a periodicity that reduces the electronic energy and impacts the physical properties of the perovskite films. Further examples and implications will be discussed in the following sections.

The observed displacements of iodine ions in multilayer perovskite films reveal an intricate interplay between the octahedral tilting and structural periodicity as a function of the layer thickness. For instance, in two- and four-layer systems, antisymmetric displacement patterns reflect a strong coupling between adjacent octahedra, where alternating shifts in opposite directions reduce strain and optimize packing, thus minimizing electronic repulsion.

This behavior suggests that octahedral tilts play a significant role in stabilizing the lattice and modulating its electronic properties, particularly through symmetry breaking effects that influence the band structure and charge transport.[18,47]

3.4. Adsorption and Interaction Energies. To explore the energetic stability of the FPEA-cation in relation to the thickness of the lowest energy configurations, we performed comprehensive analyzes focusing on adsorption (E_{ad}) and interaction energies (E_{int}). In this way, for E_{ad} we used the following equation

$$E_{ad} = (E_{tot}^{2D\ perovskite} - E_{tot}^{slab\ relaxed} - 8 \times E_{tot}^{FPEA-cation\ free})/8 \tag{5}$$

where $E_{tot}^{2D\ perovskite}$ is the total energy of the $FPEA_2(MA_{n-1})$-Pb_nI_{3n+1} perovskite thin films, in which n = 1 to 4, while $E_{tot}^{slab}{}_{relaxed}$ is the total energy of the optimized perovskite slabs through the stress-tensor without the 8 FPEA-cations adsorbates, the $E_{tot}^{FPEA-cation\ free}$ is the total energy of the free FPEA-cation and 8 is the number of FPEA removed from the slab.

For E_{int}, we computed by using the following equation,

$$E_{int} = (E_{tot}^{2D\ perovskite} - E_{tot}^{slab\ frozen} - E_{tot}^{FPEA-cation\ frozen})/8 \tag{6}$$

where $E_{tot}^{slab\ frozen}$ and $E_{tot}^{FPEA-cation\ frozen}$ are, respectively, the total energies of the frozen perovskite slab and the 8 FPEA molecules frozen in their optimized geometric positions. The results E_{ad} and E_{int} are shown in Figure 6.

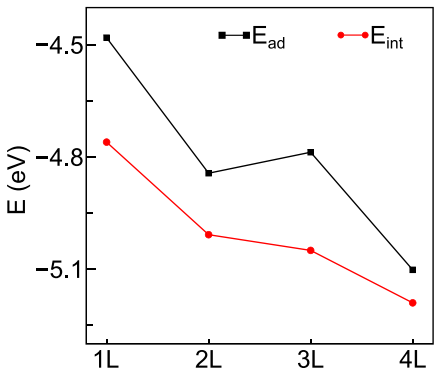

Figure 6. Adsorption (E_{ad}) and interaction (E_{int}) energies for FPEA-cations on perovskites thin films.

The results for both E_{ad} and E_{int} in all systems, n = 1 to 4, indicate that the reactions are energetically favorable (exothermic), as evidenced by the negative values. However, there are more significant differences in the values of E_{ad} between the systems compared to E_{int}. This variance can be attributed to the inherent energies of the inorganic slabs, which were optimized in the absence of FPEA molecules. As a result, these optimized slabs exhibit higher energy levels, indicating

https://doi.org/10.1021/acsaem.4c02800
ACS Appl. Energy Mater. XXXX, XXX, XXX−XXX

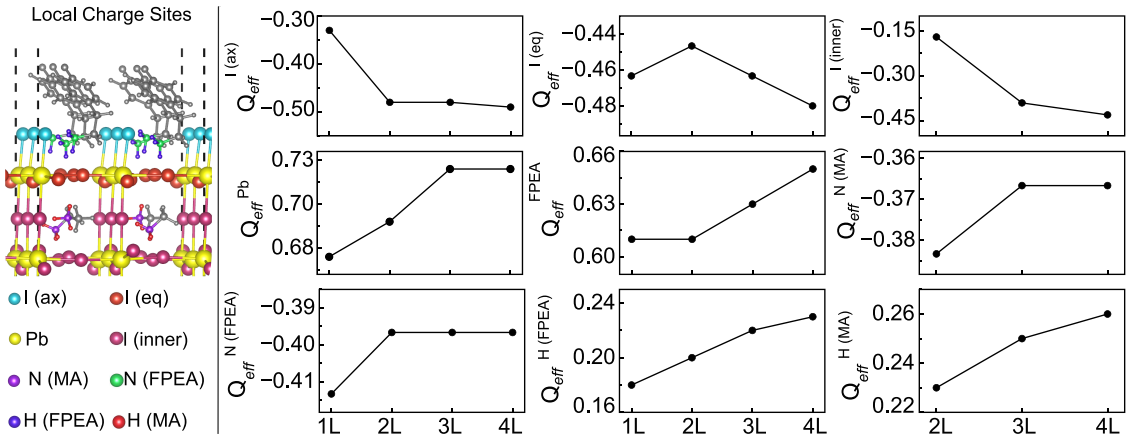

Figure 7. Effective DDEC charges for local sites: the axial ($Q_{eff}^{I(ax)}$) and equatorial ($Q_{eff}^{I(eq)}$) surface iodides and then the inner iodides ($Q_{eff}^{I(inner)}$), lead (Q_{eff}^{Pb}), nitrogen from the FPEA molecule ($Q_{eff}^{N(FPEA)}$) and the MA molecule ($Q_{eff}^{N(MA)}$), the hydrogens from NH_3^+ group, for both the FPEA molecule ($Q_{eff}^{H(FPEA)}$) and the MA molecule ($Q_{eff}^{H(MA)}$), and the charge from the FPEA molecules (Q_{eff}^{FPEA}).

greater instability. This instability contributes to the higher values E_{ad} observed in the systems, demonstrating a dependence on the parameter n.

As the thickness of the 2D system increases, we observe a notable decrease in both E_{ad} and E_{int}. Consequently, higher values of n generally correspond to more stable systems when FPEA serves as passivator cations. This finding is in good agreement with the experimental evidence. For example, Quan et al.[20] demonstrated that an increase in n leads to systems characterized by lower formation energies, particularly evident when considering the phenylethylammonium (PEA) molecule as the *P*-cation.

The robust bulky organic cations resulting from the FPEA molecules play a key role in enhancing the energetic stability of the compounds, a fact well supported by the E_{int} data. Consequently, intermolecular interactions such as van der Waals forces, H-bonds, and others emerge as crucial catalysts to augment the stability of 2D perovskites thin films.[20,48]

3.5. Effective Charge Transfer. Here we calculated the average effective charge of specific local sites from thin films using the electrostatic and chemical (DDEC) method,[35,36] the results are shown in Figure 7 at the right panel. The local sites chosen for the average effective charge analysis were: (*i*) the axial ($Q_{eff}^{I(ax)}$) and equatorial ($Q_{eff}^{I(eq)}$) surface iodides and then the inner iodides ($Q_{eff}^{I(inner)}$), (ii) lead (Q_{eff}^{Pb}), (iii) nitrogen from the FPEA molecule ($Q_{eff}^{N(FPEA)}$) and the MA molecule ($Q_{eff}^{N(MA)}$), (iv) the hydrogens from NH_3^+ group, for both the FPEA molecule ($Q_{eff}^{H(FPEA)}$) and the MA molecule ($Q_{eff}^{H(MA)}$), and finally the charge from the FPEA molecules (Q_{eff}^{FPEA}). The representative model of the local charge sites is demonstrated in Figure 7 at the left panel.

Quantum confinement effects influence the interactions of FPEA-cations with the inorganic framework, thereby affecting the charge-transfer dynamics between the organic part (positive charge) and the inorganic part (negative charge). According to the results, the percentage deviations between $Q_{eff}^{I(ax)}$ and $Q_{eff}^{I(eq)}$ tend to decrease due to the increase in the number of inorganic layers. For example, we observed deviations of 42.4% for 1L and 2.0% for 4L.

Interestingly, for 1L there is a higher concentration of charge on the equatorial iodides compared to the axial ones, precisely due to the position of the NH_3^+ group in relation to the PbI_2 plane, being more horizontal than other systems. Thus, we did not find greater deviations between $Q_{eff}^{I(eq)}$ and $Q_{eff}^{I(ax)}$ from 2L to 4L.

The effective charge on the inner iodides becomes more negative as n increases; for example, we find a difference of 0.26 e between 4L and 2L. The $Q_{eff}^{I(inner)}$ tends to approach the values found for $Q_{eff}^{I(eq)}$ and $Q_{eff}^{I(ax)}$ as the thickness of the slab increases, which could corroborate greater electronic stability for systems with larger n.

We also found that the effective charges of the monovalent (FPEA) and divalent (Pb) cations show an almost linear increase as n increases. In the case of Q_{eff}^{Pb}, there is a linear increase followed by a constant behavior after 3L. When analyzing the general average of the effective charges of the iodides, regardless of position, a consistent behavior is observed; that is, there are not many deviations on average Q_{eff}^{I} regardless of n. This leads to the hypothesis that the ionic character of the inner PbI_6-octahedra tends to increase precisely due to the difference between the average charges of Pb and I as n increases.

The role of slab thickness affects the effective charge of FPEA cations, which corresponds to a linear increase as a function of the increase in n. A more positive charge indicates more effective charge transfer through cation−anion interactions, i.e., FPEA-iodides. Furthermore, the increase in Q_{eff}^{FPEA} may be related to the greater stability of the binding energy between the organic bulky and the inorganic framework.

To have a more precise interpretation of the charge transfer behavior via FPEA cations, we investigated the effective charge of the atoms in the NH_3^+ group for both FPEA and MA molecules. The results show that $Q_{eff}^{N(FPEA)}$ for purely 2D structures (1L) has a higher concentration of negative charge, demonstrating small charge transfer to the inorganic framework. However, in quasi-2D systems (n = 2 to 4), we find a more constant character.

In fact, we have an increase in the effective charge of average hydrogen, bounded to N, as n increases. This indicates that the acidic character of the FPEA cation increases as the thickness of the slab increases, making the transfer of this hydrogen to the inorganic framework, via Brønsted−Lowry acid−base interactions, more likely.

3.6. Electron Density Difference Analysis. We conducted the electron density difference analyses to corroborate the occurrence of the charge transfer process, this validation was carried out by using the following equation

https://doi.org/10.1021/acsaem.4c02800
ACS Appl. Energy Mater. XXXX, XXX, XXX−XXX

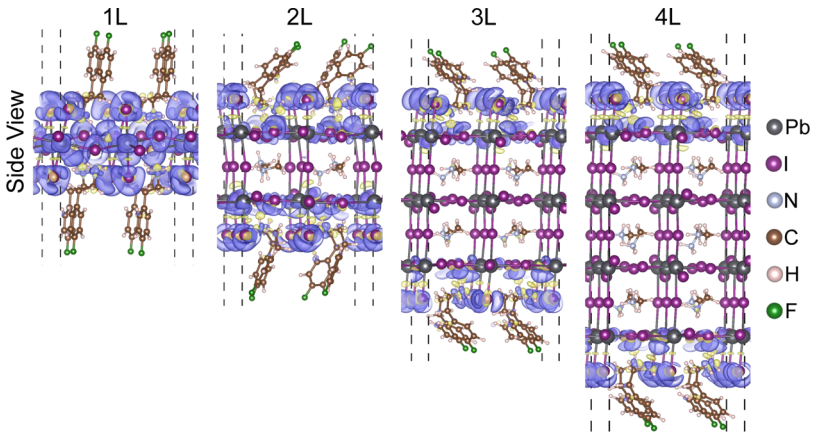

Figure 8. Electron density difference isosurfaces (0.0015 bohr^{-3}) for FPEA$_2$(MA$_{n-1}$)Pb$_n$I$_{3n+1}$ perovskites thin films, n = 1 to 4 layers. The blue and yellow regions indicate the accumulation and depletion of charge, respectively.

$$\Delta\rho = \rho^{\text{2Dperovskite}} - \rho^{\text{FPEA-cation}} - \rho^{\text{slab}} \quad (7)$$

where $\rho^{\text{2Dperovskite}}$ is the total electron density of 2D perovskites, $\rho^{\text{FPEA-cation}}$ is the electron density of the isolated bulky FPEA molecules and ρ^{slab} is the electron density of the frozen 2D slab, i.e., both are fragments obtained from the FPEA-cation/slab systems in their optimized geometric positions. The results are shown in Figure 8.

In general, we observed a large accumulation of electron charges in the neighboring I^- ion sites. Although there are charge depletions in the FPEA cations, especially in the atoms of the NH_3^+ group, this shows that the charge transfer process occurs mainly due to these chemical groups, FPEA atoms and halides. More precisely, we found charge depletions close to the H atoms of the NH_3^+ groups in both the FPEA and MA cations. We observed that there are charge depletions close to certain C atoms present in FPEA cations, especially those bounded to the aromatic ring. These depletions result from the interaction of delocalized electrons in the ring, which can be part of the charge transfer, contributing to the interaction strength between the organic and inorganic components.

3.7. Local Density of States Characterizations. To thoroughly examine the band gap energy window region, which plays a vital role in the application of perovskite materials in photovoltaic devices,[8,49] we analyzed the local density of states (LDOS). The results are illustrated in Figure 9.

LDOS analyzes were normalized in relation to the number of PbI$_6$-octahedra of each system, to facilitate comparison of densities as a function of n-layers. The results confirm the majority contributions of the PbI$_6$-octahedra to the formation of the valence band maximum (VBM) and the conduction band minimum (CBM) of the FPEA$_2$(MA$_{n-1}$)Pb$_n$I$_{3n+1}$ perovskite thin films. Specifically, we have the largest contribution coming from the iodine states, which indicates their importance for the optical properties of the systems.[50] Then we have contributions from the lead states. Thus, we have the orbital overlap of I and Pb for the formation of molecular orbitals for each hexacoordinated complex (PbI$_6$-octahedra), therefore forming the VBM and CBM of the materials.

We found small contributions of s-lead states, but significant contributions from p-iodine states to the formation of the VBM, and its formation comes from an antibonding combination of Pb ns and I p-orbitals. The VBM exhibits a high ionic character, with halides making the predominant

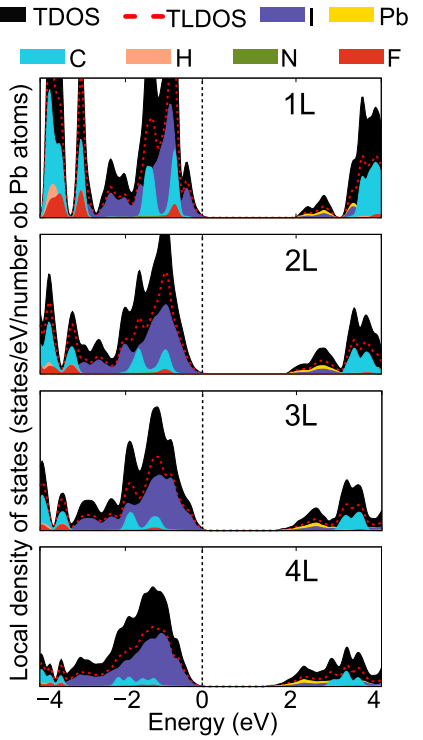

Figure 9. Local density of states for FPEA$_2$(MA$_{n-1}$)Pb$_n$I$_{3n+1}$ perovskites thin films, n = 1 to 4 layers, the valence band maximum (VBM) was set at 0 eV (vertical dashed line) and energy range considered spans from 0 to 20 eV for all plots.

contributions. This finding is consistent with previous literature.[51,52] However, the CBM shows a higher covalent character due to the increased involvement of the p states of lead and iodine.

3.8. Fundamental Electronic Band Gap. The electronic band structure for FPEA-based perovskites was calculated and is illustrated in Figure 10, here we consider calculations with and without spin−orbital coupling (SOC) effects. Due to quantum-size effects, when the thickness decreases, the CBM becomes shallower; in addition, for two- to four-layer 2D perovskite systems, we observed a break in degeneracy in the CBM region while the VBM shows smaller variations. It is noted that in the CBM for n > 2 there are greater dispersions

https://doi.org/10.1021/acsaem.4c02800
ACS Appl. Energy Mater. XXXX, XXX, XXX−XXX

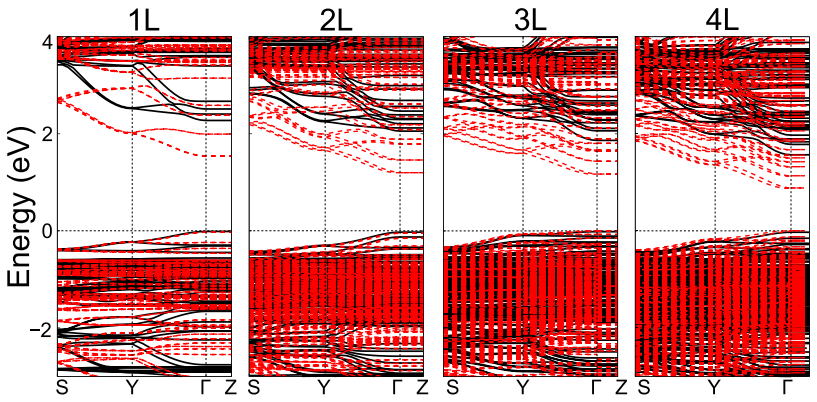

Figure 10. Electronic band structure for $FPEA_2(MA_{n-1})Pb_nI_{3n+1}$ perovskites thin films, n = 1 to 4 layers, obtained with PBE+D3 (black lines) and PBE + D3 + SOC (red lines) for the same equilibrium volume (V_0) obtained by PBE+D3 calculations. For all plots, the top of the valence band is set at 0 eV.

of bands that are also probably formed by the contributions of the states of the MA molecules between layers.

The energy difference between the VBM and CBM states delineates the fundamental band gap, (E_g). We found a direct band gap for all systems at the Γ-point. The observed values E_g consistently show a decreasing trend with increasing layer thickness, as shown in Figure 11. This phenomenon is a direct

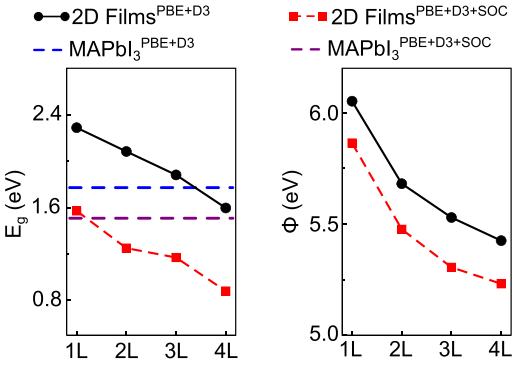

Figure 11. Electronic band gap (E_g) and the work function (ϕ) obtained by different approximations, PBE+D3 and PBE+D3+SOC, as a function of the number of n-layers for $FPEA_2(MA_{n-1})Pb_nI_{3n+1}$ perovskites thin films.

consequence of quantum-size effects, in agreement with the literature.[53,54] For instance, we found a percentage deviation of around 30% for PBE + D3 calculations, which reached 44% when considering the effects of SOC.

3.9. Work Function and Band Offset Analysis.

3.9.1. Work Function. The work function (ϕ) is defined as the minimum energy required to remove an electron from the surface of a 2D material to the vacuum region. In this work, we calculated it as the energy difference between the highest occupied state (VBM) and the electrostatic potential value in the vacuum region.[55] The ϕ outcomes are given by Figure 11.

In our previous work, we pointed out that the presence of alkaline cations with smaller ionic radii (Li, Na),[40] and also select aliphatic organic molecules such as methylammonium and propan-1-aminium,[39] can lead to a remarkable phenomenon, thickness independence ϕ. However, when molecular structures with significant polarity disparities are introduced, such as FPEA, they tend to induce pronounced deviations in the ϕ values.[56] This insight underscores the intricate interplay between molecular composition and the resulting thickness variations in ϕ.

We observed a consistent trend in the values of ϕ depending on the number of inorganic layers, n. As the number of layers increases, there is a corresponding decrease in the values of ϕ. Specifically, our results demonstrate a small deviation of 0.62 eV for the 1L compared to the 4L system. This behavior can be understood by considering that electrons in ultrathin finite materials have considerable freedom of movement along the material surface in directions a_0 and b_0, while their motion perpendicular to the material surface (c_0) is constrained and quantized, resembling a particle-in-a-box due to the presence of vacuum.[57] Thus, it becomes more energetically costly to remove electrons in systems with greater quantum-size effects, decreasing as the thickness of thin films increases.

Furthermore, the incorporation of SOC exerts discernible effects on the values of ϕ in all systems examined within this study, notably leading to a significant reduction in ϕ. For example, in the case of 3L, the effects of SOC resulted in a decrease of ϕ by approximately 4.16% from the values observed without SOC.

3.9.2. Band Offset. For a better description of the electronic structure of perovskite thin films as a function of increasing n, we analyze the band offset by aligning the VBM and CBM for all four 2D compounds by adjusting their eigenvalues with respect to the vacuum level. The band offset is shown in Figure 12. Here, we refer to the band offset considering also the SOC

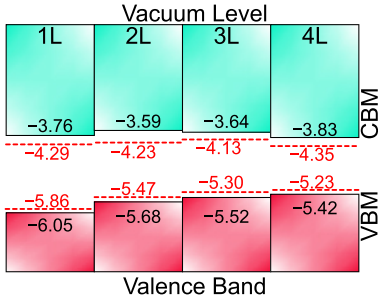

Figure 12. PBE + D3 in red VBM and green CBM for $FPEA_2(MA_{n-1})Pb_nI_{3n+1}$ perovskites thin films, n = 1 to 4 layers, in equilibrium lattice parameters with respect to vacuum level (zero energy). The red dashed line and values represent the effect of PBE + D3 + SOC calculations on VBM and CBM. All energy data here is in ev.

https://doi.org/10.1021/acsaem.4c02800
ACS Appl. Energy Mater. XXXX, XXX, XXX−XXX

effects. According to the results, we observed a greater effect of SOC on CBM for all compounds studied, shifting the bands to lower energy levels with a tendency to decrease levels from 1L to 4L. However, the CBM energy values did not exhibit any discernible trend, which can be attributed to the varied charge transfer observed from the FPEA molecules to the halides.

The most pronounced SOC effects in the CBM arise because the formation of these bands is significantly influenced by the lead−metal states, which are more susceptible to relativistic effects. In our analysis on VBM, we observed a consistent increase from the 1L to 4L systems, increasing 1.64 eV, in agreement with the expected trend of the system. This discrepancy may be attributed to the manifestation of quantum-size effects within the systems. Furthermore, our findings indicate that the increase in the VBM relative to the vacuum level demonstrates a diminishing trend as the layer count increases. This result is consistent with the data from ϕ.

3.10. Optical Properties. Understanding the intrinsic optical properties of 2D perovskite thin films is crucial for their potential applications in photonic and optoelectronic devices. Linear optical properties can be derived from the complex dielectric function as a function of frequency.[58,59] Here, we obtain the absorption spectra and refractive index of all evaluated FPEA-based perovskites.

Figure 13 (top panel) illustrates the optical absorption coefficient of $FPEA_2(MA_{n-1})Pb_nI_{3n+1}$ thin films, showing how

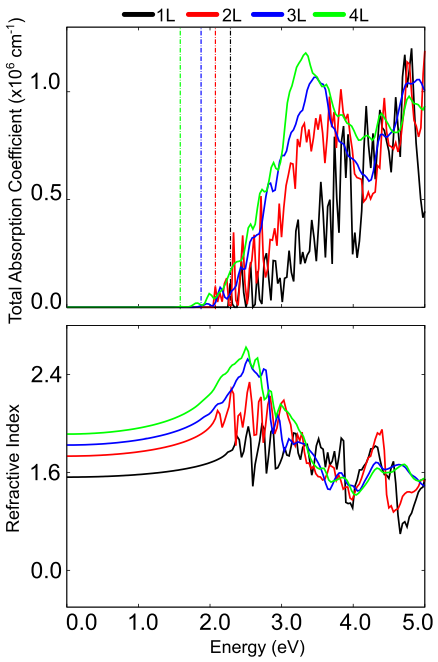

Figure 13. (top panel) Optical absorption coefficient and (bottom panel) refractive index, both obtained from PBE + D3, for $FPEA_2(MA_{n-1})Pb_nI_{3n+1}$ perovskites thin films, n = 1 to 4 layers. E_g^{optic} values are in indicated by dashed lines.

absorption evolves with increasing film thickness. A clear redshift is observed in the optical absorption edge as the number of inorganic layers increases. This trend is directly correlated with the reduction of the optical bandgap (E_g^{optic}), as indicated by the dashed lines in the figure.

The optical bandgap decreases from n = 1 to n = 4 layers, reflecting the quantum confinement effect in these materials. For thinner films with fewer inorganic layers, quantum confinement leads to an increase in the bandgap due to spatial restrictions on electronic wave functions. As the number of layers grows, the confinement effect diminishes, and the electronic states delocalize, resulting in a narrower bandgap. This is consistent with the enhanced contribution of PbI_6-octahedra to the electronic structure, as the density of states near the band edges increases with thicker layers.

These trends highlight the tunability of the optical bandgap through film thickness, which is a critical property for optimizing 2D perovskites for specific applications. For instance, a higher bandgap in thinner films makes them suitable for light-emitting applications in the blue-UV region, while lower bandgap values in thicker films are ideal for photovoltaic applications, where absorption of a broader portion of the solar spectrum is essential.

The refractive index results, shown in Figure 13 (bottom panel), further elucidate the relationship between thickness and optical properties. In the infrared region (below approximately 1.5 eV), the refractive index increases with the number of layers, which can be attributed to enhanced atomic, molecular, and bond polarizabilities. This range falls within the bandgap region, where contributions to the dielectric response are dominated by lattice vibrations and bond polarization rather than electronic excitations. The thicker films exhibit a higher dielectric response due to the increased contribution of PbI_6-octahedra, as well as the enhanced overlap of electronic orbitals. These results are consistent with experimental data, confirming the strong correlation between structural thickness and optical response.[58,60,61]

4. INSIGHTS INTO PEROVSKITES THIN FILMS THICKNESS

Quantum-size effects in perovskite thin films play a pivotal role in optimizing the performance of optoelectronic devices.[17,41] By varying the slab thickness of $FPEA_2(MA_{n-1})Pb_nI_{3n+1}$ with n-layers, we can capture these effects and gain critical insights that can assist experimentalists in fine-tuning perovskite thin films. In the following, we summarize the key findings that are particularly relevant for guiding future experimental work.

4.1. Structural Properties. Our results show that the out-of-phase distortions of PbI_6-octahedra tend to stabilize as the number of layers increases. Distortions within the inorganic framework can contribute to a reduction in charge transport. According to Chen and Choi,[62] due to the insulating nature of organic molecules, charge transport is significantly more efficient along the inorganic plane than through the organic cations. Thus, the dimensionality of the surface capping layer must be carefully adjusted, as the preferential growth of 2D perovskite crystals parallel to the substrate is not ideal for vertical charge transport in the 3D/2D perovskite film.[24] Distortions in the PbI_6octahedra can also induce exciton−phonon coupling and generate gap states, leading to a broadening of the photoluminescence spectrum.[63,64]

4.2. Energetic Stability. E_{ad} and E_{int} energies indicate greater energetic stability of the thin films as the number of n-layers increases. In fact, studies indicate that the formation energy of perovskite thin films, similar to the models evaluated, increases as the thickness decreases,[20] meaning that as the dimensionality is reduced, the energy required to form the material increases. This implies that perovskites with lower n values are less stable compared to those with higher n values. In situ methods can track 2D growth, affecting the composition of the 2D/3D interface. A higher ratio of quasi-2D phases

https://doi.org/10.1021/acsaem.4c02800
ACS Appl. Energy Mater. XXXX, XXX, XXX−XXX

improves device performance, while pure 2D layers may hinder current extraction.[65] It is known that as the value of n increases, the films tend to align vertically rather than parallel to the substrate.[66] Vertically oriented inorganic slabs provide a direct pathway for charge transport between layers, while bulky organic separators act as electrical insulators, hindering out-of-plane charge conduction.[67]

4.3. Charge Transfer. As the thickness of the slab increases, the acidic nature of the NH_3^+ groups is enhanced, which facilitates hydrogen transfer to the inorganic framework through Brønsted−Lowry acid−base interactions. This charge transfer plays a critical role in the electronic properties of the films, indicating that doping strategies or surface passivation could be used to manipulate the charge distribution and improve the electronic characteristics of the films. The doping of the organic spacers might reduce the potential barriers, thereby enhancing the charge-transport efficiency. For example, hydrogen and ionic bonding, π-π interactions, or van der Waals forces in the interlayer spaces between organic components and halogens could significantly influence the material conduction properties.[68,69]

4.4. Optoelectronic Properties. FPEA-based perovskites models act as natural quantum wells, where the PbI_6-octahedra layers are the wells and the organic cations are the barriers.[18] The barrier width is fixed by the FPEA-cation length, while the well width varies with the thickness of the inorganic layer. Therefore, as the number of inorganic layers increases, the quantum-size effects decrease and the energy gap between the valence states of the compounds (VBM and CBM) decreases. The valence states have direct contributions from PbI_6-octahedra, with larger contributions coming from the halide states and then from the divalent metal, demonstrating an ionic and antibonding character in the band gap region.

The ionic character in 2D thin films tends to decrease as the number of n-layers increases, which means that the vacancy defects created by the removal of an ion are smaller in such 2D systems, thus presenting a lower defect density.[70] The optical band gap and absorption spectra correlate with slab thickness, highlighting the role of PbI_6-octahedra in optical activity. Quantum-size effects modulate the optical properties, with absorption spectra correlating absorption intensity with inorganic layer addition. PbI_6-octahedra, especially iodides, directly influence the formation of the band gap and optical activity in 2D perovskite films. Future studies could investigate the surface defects to fully understand optoelectronic performance.

These findings underscore the importance of slab thickness and quantum-size effects on the stability, charge transfer, and optical properties of quasi-2D perovskites, offering insights into strategies for enhancing the performance of these materials.

5. CONCLUSIONS

Our DFT investigation reveals that the thickness of inorganic layers in $FPEA_2(MA_{n-1})Pb_nI_{3n+1}$ perovskite thin films significantly influences their structural, energetic, and optoelectronic properties, with quantum-size effects playing a central role. We observed that as the layer thickness increases, from 1L to 4L, the effective charge distribution between the FPEA-cations and iodides changes, enhancing charge transfer within the inorganic framework and suggesting stronger organic−inorganic interactions. This is further supported by exothermic trends in E_{ad} and E_{int}, highlighting the stabilizing impact of van der Waals forces and hydrogen bonding.

The electronic properties showed that PbI_6-octahedra dominate the valence and conduction band formation, and the optical properties of the films are closely related to these inorganic components. The absorption spectra demonstrated that the PbI_6-octahedra, particularly the iodides, are pivotal in determining the optical activity, and thicker films exhibit more intense absorption. The decreasing trend in ϕ with increasing layers underscores the influence of quantum confinement, while the effects of SOC further modulate these properties, particularly reducing ϕ. Furthermore, our findings on E_g^{optic} emphasize the critical role of PbI_6-octahedra in driving optical activity. This behavior suggests that fine-tuning the number of inorganic layers can strategically manipulate the optical and electronic characteristics of 2D perovskite films, making them highly adaptable for various optoelectronic applications.

For experimentalists, our study offers practical guidelines for optimizing quasi-2D perovskite thin films. Ensuring the vertical alignment of inorganic slabs can enhance charge transport by mitigating the insulating effects of organic cations. Surface passivation and doping strategies can further improve charge transfer and reduce defect densities. Additionally, precise control of slab thickness enables the tuning of optical properties, such as absorption edge and intensity, for targeted applications in photovoltaics and light-emitting devices.

These insights not only deepen our understanding of the role of thickness in 2D perovskite films but also highlight the importance of considering quantum-size effects and surface phenomena in designing such materials for optoelectronic applications.

■ ASSOCIATED CONTENT

Supporting Information

The Supporting Information is available free of charge at https://pubs.acs.org/doi/10.1021/acsaem.4c02800.

Data used for the figures, as well as additional analyzes and technical details (PDF)

■ AUTHOR INFORMATION

Corresponding Author

Juarez L. F. Da Silva − *São Carlos Institute of Chemistry, University of São Paulo, 13560-970 São Carlos, SP, Brazil;* orcid.org/0000-0003-0645-8760; Email: juarez_dasilva@iqsc.usp.br

Authors

Israel C. Ribeiro − *São Carlos Institute of Chemistry, University of São Paulo, 13560-970 São Carlos, SP, Brazil;* orcid.org/0000-0002-5272-8752

Felipe D. Picoli − *São Carlos Institute of Physics, University of São Paulo, 13560-970 São Carlos, SP, Brazil;* orcid.org/0000-0003-4553-0868

Pedro Ivo R. Moraes − *São Carlos Institute of Chemistry, University of São Paulo, 13560-970 São Carlos, SP, Brazil;* orcid.org/0000-0001-7339-5945

André F. V. Fonseca − *Laboratório de Nanotecnologia e Energia Solar, Chemistry Institute, University of Campinas, 13083-970 Campinas, SP, Brazil;* orcid.org/0000-0003-4098-8933

Luiz N. Oliveira − *São Carlos Institute of Physics, University of São Paulo, 13560-970 São Carlos, SP, Brazil;* orcid.org/0000-0002-4633-196X

https://doi.org/10.1021/acsaem.4c02800
ACS Appl. Energy Mater. XXXX, XXX, XXX−XXX

Ana Flávia Nogueira − *Laboratório de Nanotecnologia e Energia Solar, Chemistry Institute, University of Campinas, 13083-970 Campinas, SP, Brazil*

Complete contact information is available at: https://pubs.acs.org/10.1021/acsaem.4c02800

Funding

The Article Processing Charge for the publication of this research was funded by the Coordenacao de Aperfeicoamento de Pessoal de Nivel Superior (CAPES), Brazil (ROR identifier: 00x0ma614).

Notes

The authors declare no competing financial interest.

■ ACKNOWLEDGMENTS

The authors gratefully acknowledge the support from FAPESP (São Paulo Research Foundation, Brazil, Grant Numbers 2017/11631-2, 2018/21401-7, 2022/09312-4, 2017/11986-5, and 2023/10395-4), Shell and the strategic importance of the support given by ANP (Brazils National Oil, Natural Gas and Biofuels Agency) through the R&D levy regulation. I.C.R. thanks the National Council for Scientific and Technological Development (CNPq) for the Ph.D. fellowship, grant number 140015/2021-3. F.D.P. acknowledges financial support from the FAPESP grant numbers 2022/09312-4 and 2024/05637-1 (Ph.D. and Intership fellowship). P.I.R.M. also acknowledges financial support from the FAPESP grant number 2023/12824-0 (Postdoctoral fellowship). The authors are also grateful for the infrastructure provided to our computer cluster by the Department of Information Technology—Campus São Carlos.

■ REFERENCES

(1) Kojima, A.; Teshima, K.; Shirai, Y.; Miyasaka, T. Organometal Halide Perovskites as Visible-Light Sensitizers for Photovoltaic Cells. *J. Am. Chem. Soc.* **2009**, *131*, 6050−6051.

(2) Leng, K.; Abdelwahab, I.; Verzhbitskiy, I.; Telychko, M.; Chu, L.; Fu, W.; Chi, X.; Guo, N.; Chen, Z.; Chen, Z.; Zhang, C.; Xu, Q.-H.; Lu, J.; Chhowalla, M.; Eda, G.; Loh, K. P. Molecularly Thin Two-dimensional Hybrid Perovskites with Tunable Optoelectronic Properties Due to Reversible Surface Relaxation. *Nat. Mater.* **2018**, *17*, 908−914.

(3) Rosales, B. A.; Hanrahan, M. P.; Boote, B. W.; Rossini, A. J.; Smith, E. A.; Vela, J. Lead Halide Perovskites: Challenges and Opportunities in Advanced Synthesis and Spectroscopy. *ACS Energy Lett.* **2017**, *2*, 906−914.

(4) Yao, H.; Zhou, F.; Li, Z.; Ci, Z.; Ding, L.; Jin, Z. Strategies for Improving the Stability of Tin-Based Perovskite ($ASnX_3$) Solar Cells. *Adv. Sci.* **2020**, *7*, No. 1903540.

(5) Park, B.-w.; Kedem, N.; Kulbak, M.; Lee, D. Y.; Yang, W. S.; Jeon, N. J.; Seo, J.; Kim, G.; Kim, K. J.; Shin, T. J.; Hodes, G.; Cahen, D.; Seok, S. I. Understanding How Excess Lead Iodide Precursor Improves Halide Perovskite Solar Cell Performance. *Nat. Commun.* **2018**, *9*, No. 3301.

(6) Liu, Y.; Kim, B. J.; Wu, H.; Yuan, L.; Zhu, H.; Liu, A.; Johansson, E. M. J. Flexible Lead Bromide Perovskite Solar Cells. *ACS Appl. Energy Mater.* **2020**, *3*, 9817−9823.

(7) Frolova, L. A.; Davlethanov, A. I.; Dremova, N. N.; Zhidkov, I.; Akbulatov, A. F.; Kurmaev, E. Z.; Aldoshin, S. M.; Stevenson, K. J.; Troshin, P. A. Efficient and Stable $MAPbI_3$-Based Perovskite Solar Cells Using Polyvinylcarbazole Passivation. *J. Phys. Chem. Lett.* **2020**, *11*, 6772−6778.

(8) Min, H.; Kim, M.; Lee, S.-U.; Kim, H.; Kim, G.; Choi, K.; Lee, J. H.; Seok, S. I. Efficient, Stable Solar Cells by Using Inherent Bandgap of α-phase Formamidinium Lead Iodide. *Science* **2019**, *366*, 749−753.

(9) Yao, Z.; Zhao, W.; Liu, S. F. Stability of the $CsPbI_3$ Perovskite: From Fundamentals to Improvements. *J. Mater. Chem. A* **2021**, *9*, 11124−11144.

(10) Maniyarasu, S.; Ke, J. C.-R.; Spencer, B. F.; Walton, A. S.; Thomas, A. G.; Flavell, W. R. Role of Alkali Cations in Stabilizing Mixed-Cation Perovskites to Thermal Stress and Moisture Conditions. *ACS Appl. Mater. Interfaces* **2021**, *13*, 43573−43586.

(11) Leung, T. L.; Ahmad, I.; Syed, A. A.; Ng, A. M. C.; Popović, J.; Djurišić, A. B. Stability of 2D and quasi-2D Perovskite Materials and Devices. *Commun. Mater.* **2022**, *3*, No. 63.

(12) Stoumpos, C. C.; Malliakas, C. D.; Kanatzidis, M. G. Semiconducting Tin and Lead Iodide Perovskites With Organic Cations: Phase Transitions, High Mobilities, and Near-Infrared Photoluminescent Properties. *Inorg. Chem.* **2013**, *52*, 9019−9038.

(13) Kim, B.; Seok, S. I. Molecular Aspects of Organic Cations Affecting the Humidity Stability of Perovskites. *Energy Environ. Sci.* **2020**, *13*, 805−820.

(14) Huang, Y.; Luo, H.; Zhang, B.; Su, K.; Chen, W.; Sui, G.; Liang, L.; Zhang, B.; Song, J.; Gao, P. 2D or not 2D? Selectively Formed Low-dimensional Perovskitoids Based on Chiral Organic Cation to Passivate Perovskite Solar Cells. Appl. *Mater. Today* **2022**, *28*, No. 101550.

(15) Okumura, R.; Oku, T.; Suzuki, A.; Okita, M.; Fukunishi, S.; Tachikawa, T.; Hasegawa, T. Effects of Adding Alkali Metals and Organic Cations to Cu-based Perovskite Solar Cells. *Appl. Sci.* **2022**, *12*, No. 1710.

(16) Ruddlesden, S. N.; Popper, P. New Compounds of the K_2NIF_4 type. *Acta Crystallogr.* **1957**, *10*, 538−539.

(17) Sichert, J. A.; Tong, Y.; Mutz, N.; Vollmer, M.; Fischer, S.; Milowska, K. Z.; Garcia Cortadella, R.; Nickel, B.; Cardenas-Daw, C.; Stolarczyk, J. K.; et al. Quantum Size Effect in Organometal Halide Perovskite Nanoplatelets. *Nano Lett.* **2015**, *15*, 6521−6527.

(18) Soe, C. M. M.; Nagabhushana, G. P.; Shivaramaiah, R.; Tsai, H.; Nie, W.; Blancon, J.-C.; Melkonyan, F.; Cao, D. H.; Traoré, B.; Pedesseau, L.; Kepenekian, M.; Katan, C.; Even, J.; Marks, T. J.; Navrotsky, A.; Mohite, A. D.; Stoumpos, C. C.; Kanatzidis, M. G. Structural and Thermodynamic Limits of Layer Thickness in 2D Halide Perovskites. *Proc. Natl. Acad. Sci. U.S.A.* **2019**, *116*, 58−66.

(19) Jiang, R.; Tian, T.; Ke, B.; Kou, Z.; Muller-Buschbaum, P.; Huang, F.; Cheng, Y.-B.; Bu, T. Insights into the Effects of Oriented Crystallization on the Performance of Quasi-two-dimensional Perovskite Solar Cells. *Next Mater.* **2023**, *1*, No. 100044.

(20) Quan, L. N.; Yuan, M.; Comin, R.; Voznyy, O.; Beauregard, E. M.; Hoogland, S.; Buin, A.; Kirmani, A. R.; Zhao, K.; Amassian, A.; Kim, D. H.; Sargent, E. H. Ligand-Stabilized Reduced-Dimensionality Perovskites. *J. Am. Chem. Soc.* **2016**, *138*, 2649−2655.

(21) Hohenberg, P.; Kohn, W. Inhomogeneous Electron Gas. *Phys. Rev.* **1964**, *136*, B864−B871.

(22) Kohn, W.; Sham, L. J. Self-consistent Equations Including Exchange and Correlation Effects. *Phys. Rev.* **1965**, *140*, A1133−A1138.

(23) Zhou, Q.; Liang, L.; Hu, J.; Cao, B.; Yang, L.; Wu, T.; Li, X.; Zhang, B.; Gao, P. High-Performance Perovskite Solar Cells with Enhanced Environmental Stability Based on a (p-FC6H4C2H4NH3)2[PbI4] Capping Layer. *Adv. Energy Mater.* **2019**, *9*, 1802595.

(24) Lee, H. B.; Kumar, N.; Tyagi, B.; Ko, K.-J.; Kang, J.-W. Dimensionality and Defect Engineering Using Fluoroaromatic Cations for Efficiency and Stability Enhancement in 3D/2D Perovskite Photovoltaics. *Sol. RRL* **2021**, *5*, No. 2000589.

(25) Perdew, J. P.; Burke, K.; Ernzerhof, M. Generalized Gradient Approximation Made Simple. *Phys. Rev. Lett.* **1996**, *77*, 3865−3868.

(26) Lima, M. P.; Caturello, N. A. M. S.; Da Silva, J. L. F. Ab initio Investigation of the Interface Between $Mo_{10}S_{24}$ Nanoflakes and the Au(111) Surface: Interplay Between Interaction Energy and Morphology. *Appl. Surf. Sci.* **2022**, *604*, No. 154413.

(27) Moraes, P. I. R.; Bittencourt, A. F. B.; Andriani, K. F.; Da Silva, J. L. F. Theoretical Insights into Methane Activation on Transition-

Metal Single-Atom Catalysts Supported on the CeO_2(111) Surface. *J. Phys. Chem. C* **2023**, *127*, 16357−16366.
(28) Li, P.; Yan, L.; Cao, Q.; Liang, C.; Zhu, H.; Peng, S.; Yang, Y.; Liang, Y.; Zhao, R.; Zang, S.; Zhang, Y.; Song, Y. Dredging the Charge-Carrier Transfer Pathway for Efficient Low-Dimensional Ruddlesden-Popper Perovskite Solar Cells. *Angew. Chem., Int. Ed.* **2023**, *62*, No. e202217910.
(29) Grimme, S.; Antony, J.; Ehrlich, S.; Krieg, H. A Consistent and Accurate Ab Initio Parametrization of Density Functional Dispersion Correction (dft-d) for the 94 Elements H-pu. *J. Chem. Phys.* **2010**, *132*, No. 154104.
(30) Blöchl, P. E. Projector Augmented-wave Method. *Phys. Rev. B* **1994**, *50*, 17953−17979.
(31) Kresse, G.; Joubert, D. From Ultrasoft Pseudopotentials to the Projector Augmented-wave Method. *Phys. Rev. B* **1999**, *59*, 1758−1775.
(32) Kresse, G.; Hafner, J. Ab Initio Molecular Dynamics for Liquid Metals. *Phys. Rev. B* **1993**, *47*, 558−561.
(33) Kresse, G.; Furthmüller, J. Efficient Iterative Schemes for Ab initio Total-energy Calculations Using a Plane-wave Basis set. *Phys. Rev. B* **1996**, *54*, 11169−11186.
(34) Francis, G. P.; Payne, M. C. Finite Basis Set Corrections to Total Energy Pseudopotential Calculations. *J. Condens. Matter Phys.* **1990**, *2*, 4395−4404.
(35) Manz, T. A.; Limas, N. G. Introducing DDEC6 Atomic Population Analysis: Part 1. Charge Partitioning Theory and Methodology. *RSC Adv.* **2016**, *6*, 47771−47801.
(36) Limas, N. G.; Manz, T. A. Introducing DDEC6 atomic Population Analysis: Part 2. Computed Results for a Wide Range of Periodic and Nonperiodic Materials. *RSC Adv.* **2016**, *6*, 45727−45747.
(37) Jiang, X.; Chen, S.; Li, Y.; Zhang, L.; Shen, N.; Zhang, G.; Du, J.; Fu, N.; Xu, B. Direct Surface Passivation of Perovskite Film by 4-Fluorophenethylammonium Iodide toward Stable and Efficient Perovskite Solar Cells. *ACS Appl. Mater. Interfaces* **2021**, *13*, 2558−2565.
(38) Sahayaraj, S.; Radicchi, E.; Ziółek, M.; Ścigaj, M.; Tamulewicz-Szwajkowska, M.; Serafińczuk, J.; De Angelis, F.; Wojciechowski, K. Combination of a Large Cation and Coordinating Additive Improves Carrier Transport Properties in quasi-2D Perovskite Solar Cells. *J. Mater. Chem. A* **2021**, *9*, 9175−9190.
(39) Ribeiro, I. C.; Moraes, P. I. R.; Bittencourt, A. F. B.; Da Silva, J. L. F. Unveiling the Impact of Organic Cation Passivation on Structural and Optoelectronic Properties of Two-Dimensional Perovskites Thin Films. *Appl. Surf. Sci.* **2024**, *678*, 161098.
(40) Ribeiro, I. C.; Moraes, P. I. R.; Bittencourt, A. F. B.; Da Silva, J. L. F. Role of the Adsorption of Alkali Cations on Ultrathin n-Layers of Two-Dimensional Perovskites. *J. Phys. Chem. C* **2023**, *127*, 13667−13677.
(41) Cheng, B.; Li, T.-Y.; Maity, P.; Wei, P.-C.; Nordlund, D.; Ho, K.-T.; Lien, D.-H.; Lin, C.-H.; Liang, R.-Z.; Miao, X.; Ajia, I. A.; Yin, J.; Sokaras, D.; Javey, A.; Roqan, I. S.; Mohammed, O. F.; He, J.-H. Extremely Reduced Dielectric Confinement in Two-Dimensional Hybrid Perovskites with Large Polar Organics. *Commun. Phys.* **2018**, *1*, No. 80.
(42) Ozório, M. S.; Srikanth, M.; Besse, R.; Da Silva, J. L. F. The Role of the A-cations in the Polymorphic Stability and Optoelectronic Properties of Lead-Free $ASnI_3$ Perovskites. *Phys. Chem. Chem. Phys.* **2021**, *23*, 2286−2297.
(43) Leung, T. L.; Ahmad, I.; Syed, A. A.; Ng, A. B. Alan Man Ching Stability of 2D and quasi-2D Perovskite Materials and Devices. *Commun. Mater.* **2022**, *3*, No. 63.
(44) Cheng, B.; Li, T.-Y.; Wei, P.-C.; Yin, J.; Ho, K.-T.; Retamal, J. R. D.; Mohammed, O. F.; He, J.-H. Layer-edge Device of Two-dimensional Hybrid Perovskites. *Nat. Commun.* **2018**, *9*, No. 5196.
(45) Milot, R. L.; Sutton, R. J.; Eperon, G. E.; Haghighirad, A. A.; Hardigree, J. M.; Miranda, L.; Snaith, H. J.; Johnston, M. B.; Herz, L. M. Charge-Carrier Dynamics in 2D Hybrid Metal-Halide Perovskites. *Nano Lett.* **2016**, *16*, 7001−7007.
(46) Jahn, H. A.; Teller, E. Stability of Polyatomic Molecules in Degenerate Electronic States - I-orbital Degeneracy. *Proc. R. Soc. London, Ser. A* **1937**, *161*, 220−235.
(47) Dias, A. C.; Lima, M. P.; Da Silva, J. L. F. Role of Structural Phases and Octahedra Distortions in the Optoelectronic and Excitonic Properties of $CsGeX_3$ (x = Cl, Br, I) Perovskites. *J. Phys. Chem. C* **2021**, *125*, 19142−19155.
(48) Tyagi, P.; Arveson, S. M.; Tisdale, W. A. Colloidal Organohalide Perovskite Nanoplatelets Exhibiting Quantum Confinement. *J. Phys. Chem. Lett.* **2015**, *6*, 1911−1916.
(49) Huang, Q.; Liu, Y.; Li, F.; Liu, M.; Zhou, Y. Advances in Cesium Lead Iodide Perovskite Solar Cells: Processing Science Matters. *Mater. Today* **2021**, *47*, 156−169.
(50) dos Santos, R. M.; Ornelas-Cruz, I.; Dias, A. C.; Lima, M. P.; Da Silva, J. L. F. Theoretical Investigation of the Role of Mixed A^+ Cations in the Structure, Stability, and Electronic Properties of Perovskite Alloys. *ACS Appl. Energy Mater.* **2023**, *6*, 5259−5273.
(51) Pazoki, M.; Jacobsson, T. J.; Hagfeldt, A.; Boschloo, G.; Edvinsson, T. Effect of Metal Cation Replacement on the Electronic Structure of Metalorganic Halide Perovskites: Replacement of Lead with Alkaline-Earth Metals. *Phys. Rev. B* **2016**, *93*, No. 144105.
(52) Mosconi, E.; Umari, P.; De Angelis, F. Electronic and Optical Properties of $MAPbX_3$ Perovskites (X = I, Br, Cl): a Unified DFT and GW Theoretical Analysis. *Phys. Chem. Chem. Phys.* **2016**, *18*, 27158−27164.
(53) Wang, Z.; Lin, Q.; Chmiel, F. P.; Sakai, N.; Herz, L. M.; Snaith, H. J. Efficient Ambient-air-stable Solar Cells with 2D-3D Heterostructured Butylammonium-Caesium-Formamidinium Lead Halide Perovskites. *Nat. Energy* **2017**, *2*, No. 17135.
(54) Zhou, N.; Shen, Y.; Li, L.; Tan, S.; Liu, N.; Zheng, G.; Chen, Q.; Zhou, H. Exploration of Crystallization Kinetics in Quasi Two-Dimensional Perovskite and High Performance Solar Cells. *J. Am. Chem. Soc.* **2018**, *140*, 459−465.
(55) Shao, G. Work Function and Electron Affinity of Semiconductors: Doping Effect and Complication due to Fermi Level Pinning. *Energy Environ. Mater.* **2021**, *4*, 273−276.
(56) Shirzadi, E.; Ansari, F.; Jinno, H.; Tian, S.; Ouellette, O.; Eickemeyer, F. T.; Carlsen, B.; Van Muyden, A.; Kanda, H.; Shibayama, N.; Tirani, F. F.; Grätzel, M.; Hagfeldt, A.; Nazeeruddin, M. K.; Dyson, P. J. High-Work-Function 2D Perovskites as Passivation Agents in Perovskite Solar Cells. *ACS Energy Lett.* **2023**, *8*, 3955−3961.
(57) Da Silva, J. L. F. All-electron First-principles Calculations of Clean Surface Properties of Low-miller-index Al Surfaces. *Phys. Rev. B* **2005**, *71*, No. 195416.
(58) Song, B.; Hou, J.; Wang, H.; Sidhik, S.; Miao, J.; Gu, H.; Zhang, H.; Liu, S.; Fakhraai, Z.; Even, J.; Blancon, J.-C.; Mohite, A. D.; Jariwala, D. Determination of Dielectric Functions and Exciton Oscillator Strength of Two-Dimensional Hybrid Perovskites. ACS. *Mater. Lett.* **2021**, *3*, 148−159.
(59) Samsonova, A. Y.; Teslina, P. P.; Deribina, E. I.; Selivanov, N. I.; Stoumpos, C. C.; Kapitonov, Y. V. Low-Temperature Refractive Index Dispersion in $MAPbI_3$ Halide Perovskite Single Crystal. *J. Phys. Chem. C* **2024**, *128*, 9730−9734.
(60) Yaffe, O.; Chernikov, A.; Norman, Z. M.; Zhong, Y.; Velauthapillai, A.; van der Zande, A.; Owen, J. S.; Heinz, T. F. Excitons in Ultrathin Organic-Inorganic Perovskite Crystals. *Phys. Rev. B* **2015**, *92*, No. 045414.
(61) Guo, P.; Stoumpos, C. C.; Mao, L.; Sadasivam, S.; Ketterson, J. B.; Darancet, P.; Kanatzidis, M. G.; Schaller, R. D. Cross-Plane Coherent Acoustic Phonons in Two-Dimensional Organic-Inorganic Hybrid Perovskites. *Nat. Commun.* **2018**, *9*, No. 2019.
(62) Chen, A. Z.; Choi, J. J. Crystallographic Orientation and Layer Impurities in Two-Dimensional Metal Halide Perovskite Thin Films. *J. Vac. Sci. Technol., A* **2020**, *38*, No. 010801.
(63) Cortecchia, D.; Neutzner, S.; Kandada, A. R. S.; Mosconi, E.; Meggiolaro, D.; De Angelis, F.; Soci, C.; Petrozza, A. Broadband Emission in Two-Dimensional Hybrid Perovskites: The Role of Structural Deformation. *J. Am. Chem. Soc.* **2017**, *139*, 39−42.

https://doi.org/10.1021/acsaem.4c02800
ACS Appl. Energy Mater. XXXX, XXX, XXX−XXX

(64) Luo, J.; Wang, X.; Li, S.; Liu, J.; Guo, Y.; Niu, G.; Yao, L.; Fu, Y.; Gao, L.; Dong, Q.; Zhao, C.; Leng, M.; Ma, F.; Liang, W.; Wang, L.; Jin, S.; Han, J.; Zhang, L.; Etheridge, J.; Wang, J.; Yan, Y.; Sargent, E. H.; Tang, J. Efficient and Stable Emission of Warm-White Light From Lead-Free Halide Double Perovskites. *Nature* **2018**, *563*, 541−545.
(65) Kodalle, T.; Moral, R. F.; Scalon, L.; Szostak, R.; Abdelsamie, M.; Marchezi, P. E.; Nogueira, A. F.; Sutter-Fella, C. M. Revealing the Transient Formation Dynamics and Optoelectronic Properties of 2D Ruddlesden-Popper Phases on 3D Perovskites. *Adv. Energy Mater.* **2023**, *13*, No. 2201490.
(66) Quintero-Bermudez, R.; Gold-Parker, A.; Proppe, A. H.; Munir, R.; Yang, Z.; Kelley, S. O.; Amassian, A.; Toney, M. F.; Sargent, E. H. Compositional and orientational control in metal halide perovskites of reduced dimensionality. *Nat. Mater.* **2018**, *17*, 900−907.
(67) Mao, L.; Ke, W.; Pedesseau, L.; Wu, Y.; Katan, C.; Even, J.; Wasielewski, M. R.; Stoumpos, C. C.; Kanatzidis, M. G. Hybrid Dion-Jacobson 2D Lead Iodide Perovskites. *J. Am. Chem. Soc.* **2018**, *140*, 3775−3783.
(68) Ortiz-Cervantes, C.; Carmona-Monroy, P.; Solis-Ibarra, D. Two-Dimensional Halide Perovskites in Solar Cells: 2D or not 2D? *ChemSusChem* **2019**, *12*, 1560−1575.
(69) Blancon, J.-C.; Stier, A. V.; Tsai, H.; Nie, W.; Stoumpos, C. C.; Traoré, B.; Pedesseau, L.; Kepenekian, M.; Katsutani, F.; Noe, G. T.; Kono, J.; Tretiak, S.; Crooker, S. A.; Katan, C.; Kanatzidis, M. G.; Crochet, J. J.; Even, J.; Mohite, A. D. Scaling law for excitons in 2D perovskite quantum wells. *Nat. Commun.* **2018**, *9*, No. 2254.
(70) Xue, H.; Chen, Z.; Tao, S.; Brocks, G. Defects in Halide Perovskites: Does It Help to Switch from 3D to 2D? *ACS Energy Lett.* **2024**, *9*, 2343−2350.

https://doi.org/10.1021/acsaem.4c02800
ACS Appl. Energy Mater. XXXX, XXX, XXX−XXX